STAFF SUMMARY SHEET

	TO	ACTION	SIGNATURE (Surname), GRADE AND DATE		TO	ACTION	SIGNATURE (Surname), GRADE AND DATE
1	DFAN	sig	REED, SHAD Lt Col 26JULY13	6			
2	DFER	approve	Add Distro Statement to Paper (Some types) 29July	7			
3	DFAN	action	(Author /Originator)	8			
4				9			
5				10			

SURNAME OF ACTION OFFICER AND GRADE	SYMBOL	PHONE	TYPIST'S INITIALS	SUSPENSE DATE
McLaughlin, CIV		333-2613	caf	20130730

SUBJECT		DATE
Clearance for Material for Public Release	USAFA-DF-PA-414	20130724

SUMMARY

1. PURPOSE. To provide security and policy review on the document at Tab 1 prior to release to the public.

2. BACKGROUND.
Authors: Casey Fagley, Chris Porter, Tom McLaughlin

Title: Predictive Flow Control to Minimize Convective Time Delays

Circle one: Abstract Tech Report (Journal Article) Speech Paper Presentation Poster

Thesis/Dissertation Book Other: _____

Check all that apply (For Communications Purposes):

[ ] CRADA (Cooperative Research and Development Agreement) exists

[] Photo/ Video Opportunities [] STEM-outreach Related [] New Invention/ Discovery/ Patent

Description: This paper shows a methodology for minimizing inherent convective time delays in fluid systems by using a class of model predictive control. The methodology is applied to the ogive at high angle of attack. Results show that model predictive control becomes highly sensitive to unmodeled non-linearities or varying time delays, as expected.

Release Information: The paper will be presented at the AIAA Guidance, Navigation and Control Conference

Previous Clearance information: (If applicable)

Recommended Distribution Statement: Distribution A: approved for public release, distribution unlimited

3. DISCUSSION.

4. RECOMMENDATION. Sign coord block above indicating document is suitable for public release. Suitability is based solely on the document being unclassified, not jeopardizing DoD interests, and accurately portraying official policy.

//signed//
THOMAS E. MCLAUGHLIN, Ph.D.
Director, Aeronautics Research Center

Predictive Flow Control to Minimize Convective Time Delays

Casey Fagley*, Chris Porter† and Thomas McLaughlin‡
Department of Aeronautics, U.S. Air Force Academy, USAF Academy, CO 80841, USA

To overcome the convective time delay issue for active closed-loop flow control, a model based predictive control algorithm is analyzed. From a controls perspective, forms of internal model control or model predictive control can be used to accommodate and minimize the effect of systems with pure time delays. Moreover, the Smith predictor is a commonly employed control technique to negate the pure time delay in a closed-loop system. This form of model predictive control is applied to the asymmetric vortex problem of an axisymmetric forebody (specifically a von Kármán ogive with fineness ratio of 3.5) at high angle of attack ($\alpha = 50°$). Full order Navier-Stokes are numerically solved and provide the plant process. Small port and starboard blowing patches are used to introduce fluidic disturbances at the nose of the ogive to augment the global flow state and produce a deterministic vortex state. As the active flow control technique exploits the convective instability, a convective time delay exists. Linear-time-invariant and non-linear time invariant models are developed from the open-loop dynamics. A Smith predictor is employed within the full order CFD simulation. The results of the predictive control are compared to open-loop and model-free closed loop behavior. It is shown that the predictive control developed in this paper while very suitable for control of this type of flow is very sensitive to modeling uncertainties.

Nomenclature

A	Base area	$\hat{V}$	Velocity vector
C	Linear observation matrix	P	Pressure
$\hat{C}_y$	Estimated side force coefficient	Re	Reynolds number, $U_\infty D/\nu$
C_P	Pressure coefficient	t	Time
D	Diameter	U	Freestream velocity
D	Diameter	u_1, u_2	Reduced-order model inputs
D	Base diameter	U_∞	Free-stream velocity
f_r	Fineness ratio, L_{cone}/D	$\mathbf{x_s}$	Surface pressure sensor location
L	Length of the ogive model		
L	Model length	α	Angle of attack
L_{aft}	Aft body length	ΔC_P	Differential pressure coefficient, port - starboard
L_{cone}	Nose cone length		
M	Mach number	θ	Circumferential angular position
$K_p, T_z, \zeta, T_w, T_d$	Reduced-order model parameters	ρ	Density
$\hat{n}$	Normal vector	τ	Convective time

I. Introduction

RESEARCH in *closed-loop flow control* is attempting to improve the performance and robustness of control strategies for highly, non-linear complex flow fields. Due to natural instabilities in fluid flows, closed-loop flow control has the potential to improve performance of all engineering systems in which a fluid flows, e.g. external flows around air vehicles or ground based systems such as bridges and buildings, internal flows in pipes and propulsion systems, acoustical emission and mitigation, combustion and mixing problems, turbulence and transition management, as well as alternative energy applications such as wave and wind power devices. Flow control can be categorized into two approaches, passive and active. Passive flow control makes use of geometry modifications to alter the mean fluidic behavior to produce a desired effect. A classic example of passive control is the dimples on a golf ball to transition the boundary layer, thus delaying separation and reducing pressure drag. Another example from airplane aerodynamics is the boundary layer fences on wings that ensure that longitudinal vortices are created and delay flow separation at high angles of attack. Such passive flow control strategies are based on a quasi-steady flow assumption and have been extensively studied in the past.

In contrast, active flow control, which introduces a small amount of energy to the flow (e.g. momentum addition, mass addition, vorticity addition), allows for direct, local, and instantaneous modification of the flow field. The most efficient way to employ active flow control is to exploit natural instabilities in the flow field, which allows for a minimal actuation effort. A perturbation is introduced into the flow and is amplified through the fluidic

*Research Associate, Department of Aeronautics, Member
†NRC Associate, Department of Aeronautics, Member
‡Director, Aeronautics Research Center, Department of Aeronautics, Associate Fellow

— Add Distribution Statement

instability as the disturbance convects downstream in the flow field; this phenomenon is commonly referred to as a convective instability. Analyzing published active flow control efforts, a number of technical challenges can be identified. In large, the temporal delay due to the time necessary for a perturbation to convect and grow to a significant size to effect the global flow state provides a challenging problem. Recent research in fluidic actuator development (e.g. synthetic jets, plasma actuators, vortex generators) provide very responsive dynamics such that convective time delays become the limiting factor in terms of closed-loop system performance, thus model-free based control approaches will not yield the best performance.

To overcome the convective time delay issue, a model which captures the dynamics is essential for predictive control. Fluid flows exhibiting exploitable instabilities are governed by the Navier-Stokes equations, a set of second-order, non-linear partial differential equations. Unfortunately, the complexity of the governing equations provides little to no insight for classical or modern control design theory. Also, control theory is very limited when faced with high-dimensional, extremely non-linear systems. A proven way to reduce the dimensionality of the problem while still capturing the essential system dynamics of a flow problem is through reduced order models (ROMs), where a given model of a system or process is replaced by a smaller approximation to the original model. The identified ROM can then be used as a predictive model to minimize the time delay through the system.

In control theory time delay issues are a common problem to overcome. Forms of internal model control or model predictive control can be used to accommodate and minimize the effect of such issues. In particular, Smith predictors are commonly used in systems with pure time delays. In essence the Smith predictor is broken up into two loops, one of which computes control of the delay free model using a primary controller (typically a proportional integral derivative control), while the other, minor loop, eliminates the actual delayed measurement; thus, the closed-loop frequency response can be increased beyond the performance of standard, model-free approaches. The downside of implementing a Smith predictor is any model uncertainty in terms on non-linear behavior, inaccurate time delays, or varying time delays drastically hinders the performance of the predictive control.

This paper uses a model based smith predictor to control a non-linear fluid dynamic problem. The predictive control results are compared to that of the open-loop behavior and a standard model-free, control approach.

A. Flow Field

The flow field around a slender, axisymmetric forebody varies dramatically with the angle of attack. Typically, four flow regimes are observed: attached flow ($0° \leq \alpha < 15°$), symmetric vortex flow ($15° \leq \alpha < 40°$), asymmetric vortex flow ($40° \leq \alpha < 60°$), and unsteady wake-like flow ($\alpha \geq 60°$) [1–3]. Illustrations of these flow regimes are shown Fig. 1. The transition between the symmetric and asymmetric vortex flow is due to an instability of the natural flow field. Minor geometric imperfections and flow perturbations are amplified by this convective instability and divert the flow field away from the symmetric vortex state into an asymmetric vortex state in which either port or starboard vortex will separate from the forebody surface and cause a large asymmetric pressure distribution on the ogive surface.

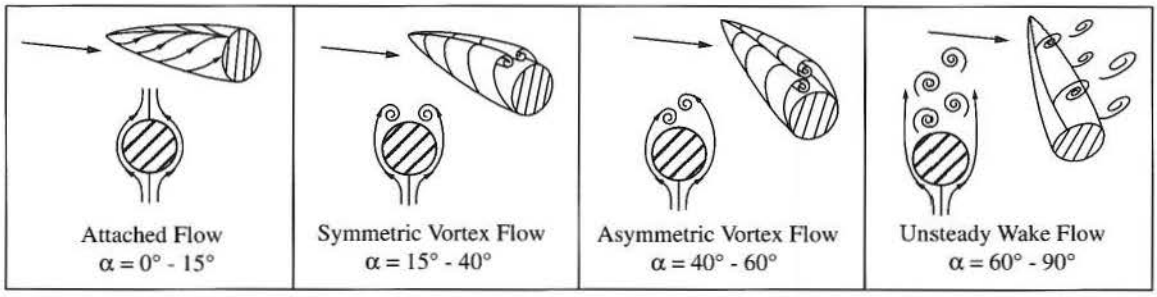

Figure 1. Flow state on a tangent-ogive forebody as a function of angle of attack.

Once this occurs, the asymmetric vortex state produces a significant side force on the body, typically on the order of 40% to 70% of the normal force depending on angle of attack. This side force or phantom yaw is a detrimental problem for the stability and maneuverability characteristics of slender flight vehicles at high incidence [4–6]. Numerous experimental and numerical investigations for a range of geometric shapes and Reynolds numbers have been performed to understand this phenomenon.

The natural tendency of the flow field to favor an asymmetric vortex state emphasizes the importance of forebody vortex management. A variety of different flow control methods have been devised for different forebody configurations. Typically, passive control techniques, in which no energy is added to the flow, make use of nose strakes, dimples, nose blunting, and other geometric modifications to reduce the flow's instability and enforce a symmetric vortex state [4, 7, 8]. To improve vortex management performance with respect to passive techniques and open-loop methods, closed-loop active flow control, in which sensor signals are used to estimate the flow

state and then prescribe the actuation input to reach a desired state, hold the promise to increase stability and maneuverability characteristics for high angles of attack at varying flow conditions. Active closed-loop flow control presents the opportunity to not only regulate side force, but also allow for the possibility to attain attitude control of a slender body via active vortex manipulation.

To date very little research has been performed to exploit the full potential of feedback flow control on axisymmetric forebodies. Bernhardt and Williams [9] focused on regulating the side force over a range of angles of attack through the use of active closed-loop control using both PID and artificial neural network-PD control. The overall results of their control effectiveness is shown in Fig. 2a. As shown, their controller was able to effectively manage the asymmetric vortex state, all but eliminating any side force and yawing moment up to an angle of attack of 48°. According to the report, the highly unstable oscillatory response at increasing angles of attack exceeded the bandwidth of actuator hardware and therefore hindered controller performance at higher angles of attack. Secondly, Patel et al. [10] were also able to successfully close the loop on an axisymmetric forebody by employing deflectable tabs to manipulate the vortex state and achieve a desired side force and yawing moment. However, the use of deflectable tabs also resulted in slow actuation changes and potentially increased the drag on the model (Fig. 2b).

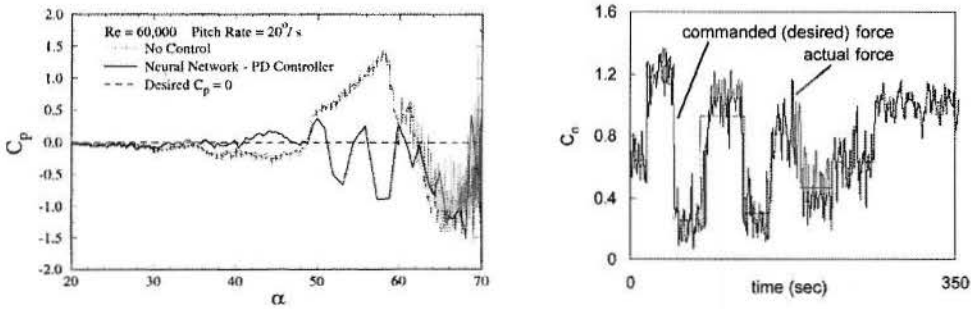

a) Closed-loop results from Bernhardt et al. [11]

b) Closed-loop results from Patel et al. [10]

Figure 2. Previous experimental closed-loop flow control results of an axisymmetric forebody at high angles of attack. [9–12]

Also, closed-loop experimental results from the US Air Force Academy [13] which implemented plasma actuation, surface mounted pressure sensors and a PID control algorithm show the ability to reference track quasi-steady side force set points. The unsteady fluctuations (from the separated shear layer along the bluff body) are unable to be reduced, as shown in Fig (??). Because plasma actuators have very responsive dynamics, the lack of the ability to reduce the unsteady fluctuations proved that it's not associated with actuator dynamics, but rather convective time delays, as the closed-loop bandwidth was only limited by the response of the asymmetric vortex state due to an introduced disturbance at the nose of the ogive and propagation time of the disturbance.

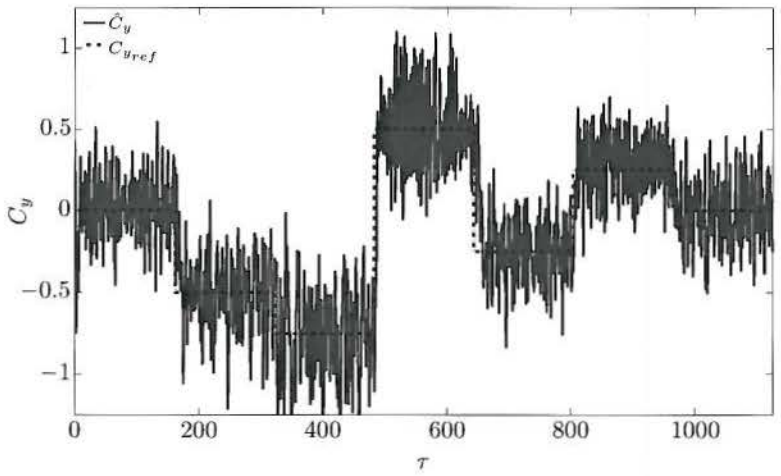

Figure 3. Time history of closed-loop test with the reference side force, $\hat{C}_{y_{ref}}$, in dotted black and estimated side force, $\hat{C}_y$, shown in blue. [13]

II. Setup

A. Simulations

The geometry considered in this investigation is a generic von Kármán ogive which is a part of the Haack series nose cones with fineness ratio $f_r = 3.5$ and a diameter of $D = 0.1$ m. The nose cone shape is computed from Eq (1) and (2), where the origin of the coordinate system is at the nose of the model.

$$\theta_o = \arccos\left(1 - \frac{2x}{L_{cone}}\right) \tag{1}$$

$$r = \frac{D\sqrt{\theta_o - \frac{\sin(2\theta_o)}{2} + C\sin^3\theta_o}}{2\sqrt{\pi}} \tag{2}$$

A cylindrical aft body with length $L_{aft} = 0.05$ m is added to the end of the ogive forebody. Figure 4 shows the geometry used in both the experiment and simulation.

The CFD solver used is Cobalt, an unstructured finite-volume code developed for the solution of the compressible Navier-Stokes equations. The basic algorithm is described in Strang et al., although substantial improvements have been made since then [14]. The numerical method is a cell-centered finite volume approach applicable to arbitrary cell topologies (e.g, hexahedra, prisms, tetrahedra). The spatial operator uses a Riemann solver, least squares gradient calculations using QR factorization to provide second order accuracy in space. A point implicit method using analytic first-order inviscid and viscous Jacobians is used for advancement of the discretized system. For time-accurate computations, a Newton sub-iteration scheme is employed, resulting in a method that is formally second order accurate in time. For parallel performance, Cobalt utilizes the domain decomposition library ParMETIS to provide optimal load balancing with a minimal interface between zones [15].

To compute the flow around the model, an unstructured grid was generated which contained 16 million total elements. Near the surface of the body, a boundary layer grid was used to provide a dense spacing of grid points near the model due to the sensitivity of the flowfield to small disturbances. A spherical farfield boundary was placed 40 model diameters away from the origin to minimize the influence of possible pressure reflections. A schematic of the model geometry, used in the accompanying experiment, and replicated computationally is shown in Fig. 4.

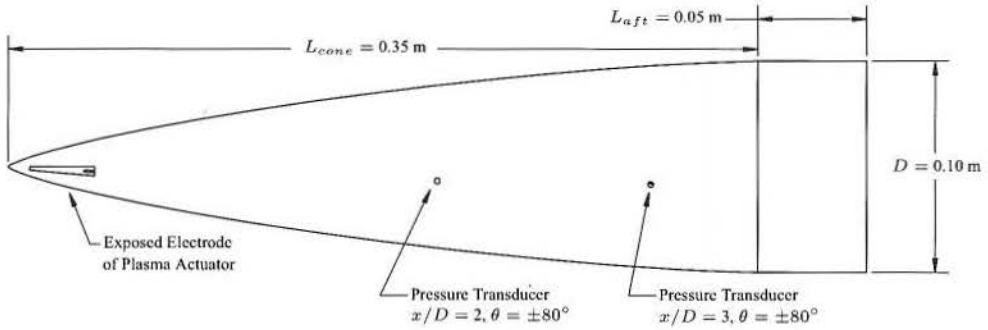

Figure 4. Schematic drawing of experimental axisymmetric forebody. The pressure transducer locations [16] and plasma plasma actuators are shown.

The experiment employed two single dielectric barrier discharge plasma actuators at the tip of the ogive to augment the flow field as described in Fagley et al. [?]. To replicate this actuation mechanism within the CFD simulation, two user-specified, mass-blowing patches were placed at $\pm 90°$ from the windward meridian, 1 cm downstream from the tip of the model. These patches were 2 cm long with a width of 0.015 cm. The mass-blowing patches were set to blow at $\delta = 30°$ (Fig. 5a) to mimic the plasma actuators in the accompanying experiment [17]. Finally, a small pin shaped disturbance was added at 90° to the starboard side of the model. The pin had a diameter of 0.01 cm and was 0.0045 cm tall. The center of the pin was placed 0.4 cm downstream from the tip of the model. The pin provided an initial geometric disturbance to initiate a natural, deterministic asymmetric vortex state. Figure 5a shows a zoomed in view of the tip of the model, showing the pin and the actuator design.

Surface mounted pressure transducers were placed in the ogive to estimate the instantaneous side force, because realtime force measurements are susceptible to frequency responses which are limited to the inertia of the body and are not feasible in actual application. The locations of the pressure transducers are shown in Figure 4. The sensor placement was determined through an optimal genetic algorithm as documented by Fagley et al. [16]. This arrangement of sensors minimized the linear estimation between the four pressure transducer measurements

and side force measurements in forced and unforced CFD simulations. The estimated force is computed by the linear model,

$$\hat{C}_y(t) = CP(\mathbf{x_s}, t). \tag{3}$$

where $P(\mathbf{x_s}, t)$ is the array of pressure measurements at surface locations x_s, C is the vector of coefficients which map pressure measurements into the estimated side force, C_y. The port side plasma actuator is also shown in Figure 4. Detailed information on the fabrication, implementation and open loop performance of the SDBD plasma actuator can be found in [18].

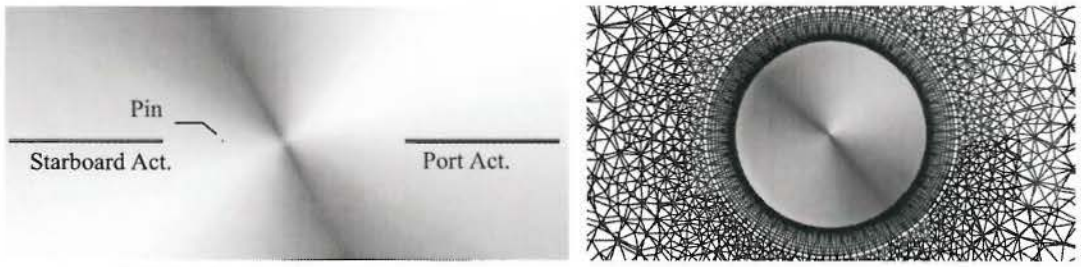

a) Starboard and port mass blowing slots

b) Cross-sectional view of the grid at $X/D = 2$.

Figure 5. Starboard and port mass blowing slots shown in (a) along with front (b) view of the computational grid used. The grid contains $6,711,157$ nodes and $15,568,273$ elements.

III. Results

All of the figures and data presented are normalized by the convective flow through time for the free stream velocity as given by,

$$\tau = \frac{tU_\infty}{L}, \tag{4}$$

with the corresponding convective frequency,

$$f_\tau = \frac{L}{tU_\infty}. \tag{5}$$

To characterize the effectiveness of the actuator within the CFD simulation the non-dimensional momentum coefficient given by,

$$\mathrm{C}_\mu = \frac{|\int_A \rho \hat{V}(\hat{V} \cdot \hat{n}) dA|}{\rho_\infty U_\infty^2 A}, \tag{6}$$

was used.

A. Approach

To reduce the effect of convective time delays, the closed-loop response time is minimized. For this a modified smith predictor is implemented to increase the crossover frequency and phase margins of the closed-loop system. The chosen control structure is shown in Figure 6. This controller uses a linear model without the pure time delay as a future predictor of the plant response to improve upon controller responsiveness. The measured output is then negated by the delayed model response, thus if the plant is exactly equal to the model the pure time delay can be accounted for. The control algorithm or compensator ($G_c(s)$), is typically a proportional - integral - derivative algorithm. The advantage is such that the error term, or control input, now operates on an estimated model response at a convective flow through time advancement.

To implement this type of predictive control, a model is now necessary of the underlying physical dynamics. The system response was modeled using a linear system parameterization. The input-output relationship for this system is given by,

$$Y(s) = G_s(s)U(s). \tag{7}$$

The structure of the model in continuous time has the form,

$$G_s(s) = \frac{N(s)}{D(s)} = Ke^{\theta s}\frac{s^m + a_{m-1}s^{m-1} + a_{m-2}s^{m-2} \cdots a_1 s + a_0}{s^n + b_{n-1}s^{n-1} + b_{n-2}s^{n-2} \cdots b_1 s + b_0} \tag{8}$$

for a linear system with m zeros, n poles, and a pure time delay, $e^{\theta s}$. A pure time delay is necessary because of the physical convective time from which a disturbance is introduced to the flow and reaches the sensing location.

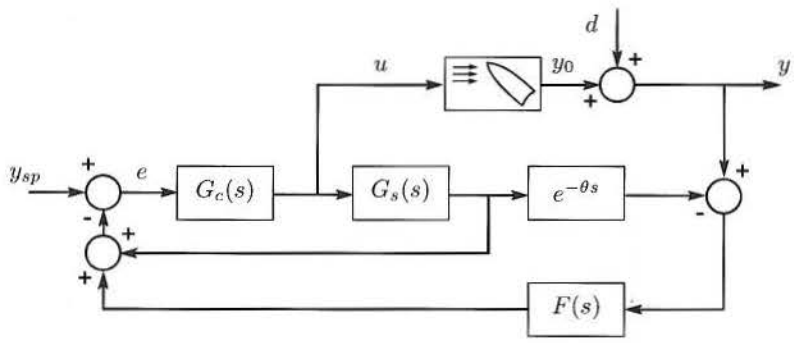

Figure 6. Smith predictor control structure for control of asymmetric state on a von Kármán Ogive

Different system identification techniques exist for parameterizing suitable models $G(s)$, determining the polynomial orders m and n, and solving for the coefficients of the polynomials in the numerator and denominator. The technique for time domain identification used in this effort is the Prediction Error Method (PEM). The PEM technique is an iterative approach to determining a minimum error, in a least squares sense, for a selected model structure given by an autoregressive moving average (arma) system. This approach works in the continuous and discrete time domains and is applicable for multi-input multi-output time domain data sets. The PEM technique directly identifies with a model structure of the form of Eq. (8). In particular, a model structure as shown in (9) was suitable for capturing the temporal dynamics due to a step input.

$$G_s(s) = K_p \frac{1 + T_z s}{(1 + 2\zeta T_w s + (T_w s)^2)} e^{-T_d s}. \tag{9}$$

Because high-fidelity CFD simulations are CPU demanding and take on the order of 60 hours for a single simulation, this does not allow for an amenable environment for control algorithm design and tweaking. Therefore, an intermediate, non-linear model must be developed to simulate the closed-loop dynamics. Previous results show that three forcing regimes exist. At lower forcing magnitudes of C_μ, the jet actually create a separation bubble which accelerates the flow, delaying separation and causing an attached vortex. At medium forcing magnitudes, the jet induces separation causing a detached vortex, and at highest forcing magnitudes, the jet produces a coanda like effect and causes an attached vortex state [19]. Thus, for the purposes of this paper, only forcing magnitudes which induce separation, or induce a detached vortex are considered because the largest range of side force magnitudes are attained in this forcing regime. In this forcing regime, although the temporal dynamics due to a step input are relatively constant, the steady-state response of side force is non-linear as shown below in Fig 8a.

A Hammerstein-Wiener model structure (NLHW) was selected. This model structure applied a nonlinear function to both the inputs and outputs of a linear model. The NLHW model was built using sigmoidnets to account for the input nonlinearity and wavenets to account for the output nonlinearity. Furthermore, the model was trained using only the open-loop data, and validated against the closed-loop data. To determine the number of sigmoidnets and wavenets needed, the model was trained allowing each to vary from one to ten, and the average fit-error across all the data sets was calculated, including the closed-loop data. The final results indicated that eight sigmoidnets and four wavenets provided the best fit to the data. This creates a black-box model structure built solely for the purposes of data replication, such that it provided an accurate model for controller development. The results of a step-input in forcing as well as the steady-state response are also shown in Fig. ??.

B. Transient Dynamics

To model the system dynamics of the asymmetric vortex state behind the von Kármán ogive at high angles of attack, open-loop CFD simulations were conducted to understand system characteristics in terms of stability/bi-stability, controllability, observability, and linear/non-linear behavior. The flow behind an axisymmetric slender body has previously been shown to be completely bistable at a sufficiently large angle of attack and small Reynolds numbers. Because few tests have been conducted at a Reynolds number in the range of the current simulation (Re = 156,000) with this unique geometry, determining if a bi-stable or proportional flow regime exists is critical in designing a suitable model structure and control system design.

The open-loop dynamics are determined purely from step and impulse actuation inputs. The step inputs were varied at different actuation inputs in terms of plasma voltages and blowing coefficients for the experiments and simulations, respectively. The impulse input was varied over a range of flow through times. Figure 7a shows the comparison of the step response for the experimental measurements of the side force, the numerical simulation and the model estimation. Both of the numerical and experimental data were offset so that the initial

state was zero. As shown, the agreement is very good among experimental, numerical and model response. The step input data ensemble served for the training data for which the linear model was fit. Figure 7b shows the experimental, numerical and model responses to an impulse response which varied with duty cycle by percentages of the normalize flow through time. The impulse data set served as the validation for the model verification. Very good agreement between all three systems existed.

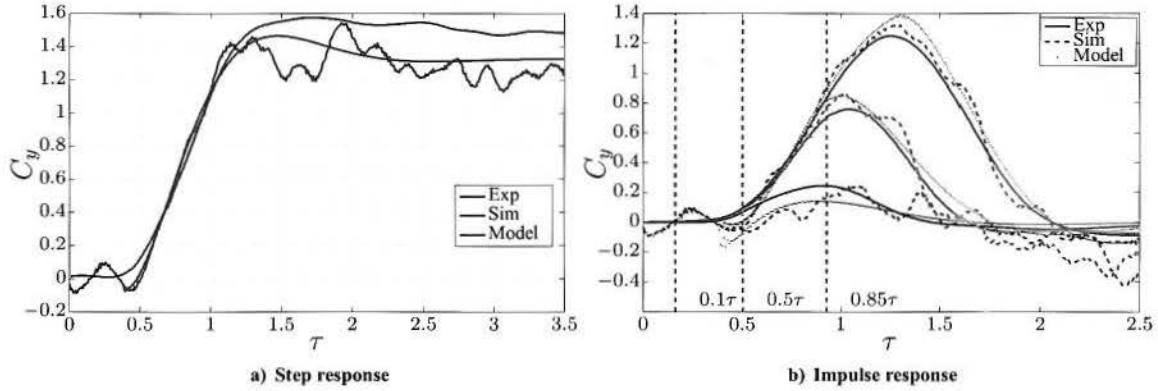

a) Step response b) Impulse response

Figure 7. a) Step response for experiment [blue], simulation [green], and LTI model prediction [model]. b) Impulse response for experiment[-], simulation[–], and LTI model [.] at varying percentages of τ.

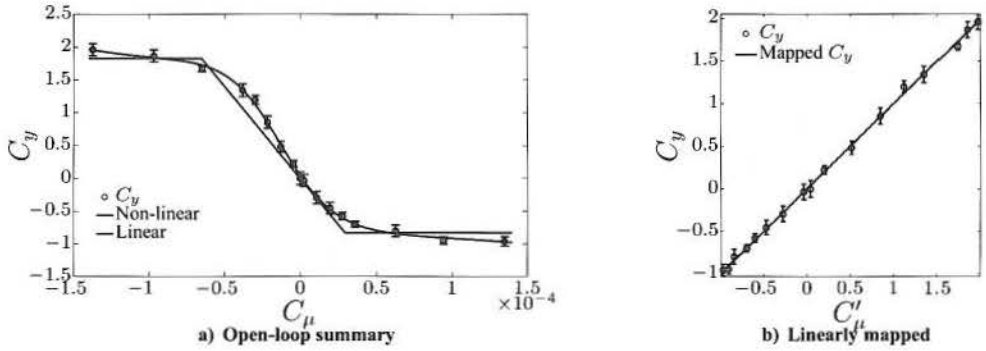

a) Open-loop summary b) Linearly mapped

Figure 8. a) Open-loop summary for steady state response of C_y due to step input of C_μ (positive starboard forcing and negative port forcing), linear and non-linear representations also plotted. b) Conformal mapping of $C_\mu \rightarrow C'_\mu$ using a rational polynomial best fit.

C. Closed-Loop Results

The LTI model developed above provides a relationship between the input momentum coefficient and the resultant estimated side force. To compare the results of a predictive control, a simple, model-free controller was initially developed. A proportional-integral controller, $G_c(s) = K_p + K_i/s$, was selected to close the loop.

such that the dynamics of a closed-loop controller can be evaluated. A schematic of the feedback system implemented is shown in Fig. ?? and formulated in Eq. (10),

$$Y = \begin{bmatrix} \frac{G_s G_c}{1+G_s G_c} & \frac{1}{1+G_s G_c} \end{bmatrix} \begin{bmatrix} r \\ d \end{bmatrix}, \tag{10}$$

where r and d are the reference and disturbance inputs, respectively.

With the system shown in Eq. (10) , the transfer function between different input-output pairs can be analyzed for various forms of $G_c(s)$. As an initial control design, a standard PI controller for $G_c(s)$ was implemented,

$$G_c(s) = K_p + \frac{K_i}{s} \tag{11}$$

where K_p and K_i are the proportional and integral terms, respectively. No derivative gain was used since the derivative term resulted in an instability in the transfer function, $G_s G_c/(1 + G_s G_c)$, purely due to the time delay in the system. The gains, K_i and K_p, were selected to achieve high fluidic response times while maintaining adequate stability margins. As shown in Fig. ??, the open-loop phase margin is 65° and the open-loop gain margin is 1.63 or 5 dB.

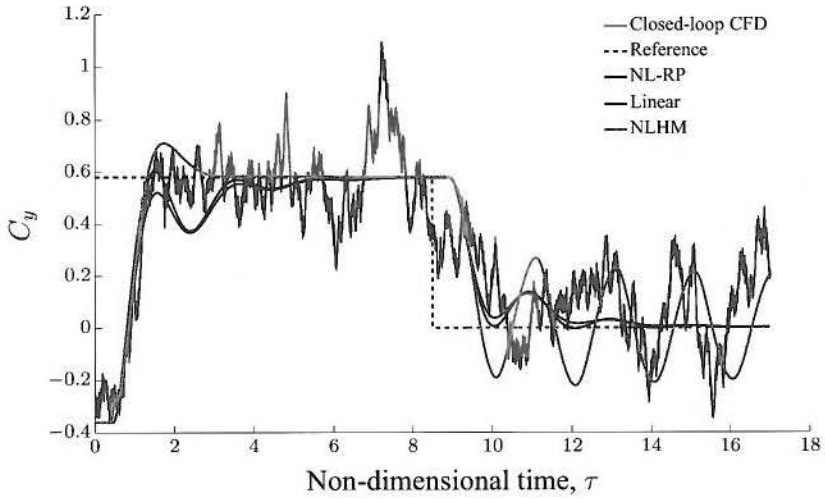

Figure 9.

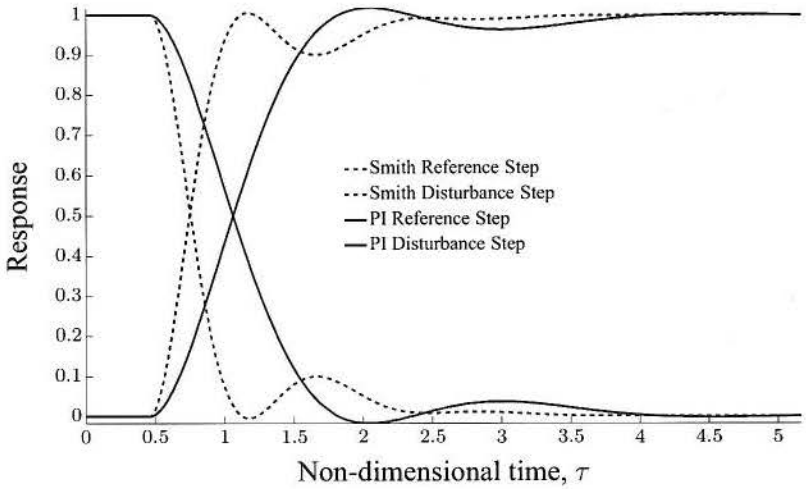

Figure 10.

IV. Conclusion

The asymmetric vortex regime of a axisymmetric bluff body with a fineness ratio of 3.5 is experimentally and computationally studied at a Reynolds number of 156,000. Both port and starboard plasma actuators are used to introduce fluidic disturbances at the tip of the ogive in the experimental setting. Mass blowing ports which introduced momentum in the flow were used in the simulations. These disturbances are amplified through the flow's convective instability to produce a deterministic port or starboard asymmetric vortex state (i.e. side force). Accurate control or manipulation of this asymmetric vortex phenomenon holds the potential for increased maneuverability and stability characteristics of slender flight vehicles.

Unforced and open-loop experimental tests were carried out to understand and quantify the vortex dynamics. Step and impulse inputs provided the necessary dynamics and diverse training and validation data sets for the formulation of a linear time invariant dynamical model. Standard linear system identification approaches were implemented to represent the training data set. In particular prediction error was used to capture the asymmetric vortex dynamics. These methods were validated by time and frequency domain methods. The measurements and modeling methods showed the cutoff frequency of the flow to be around two flow through times, i.e. the time it takes a particle to flow from the tip of the model to the base of the ogive section.

A closed-loop system was designed such that the unforced fluid dynamics and measurement noise were modeled as an output disturbance. The prediction error model was well suited for this system. A PID controller was

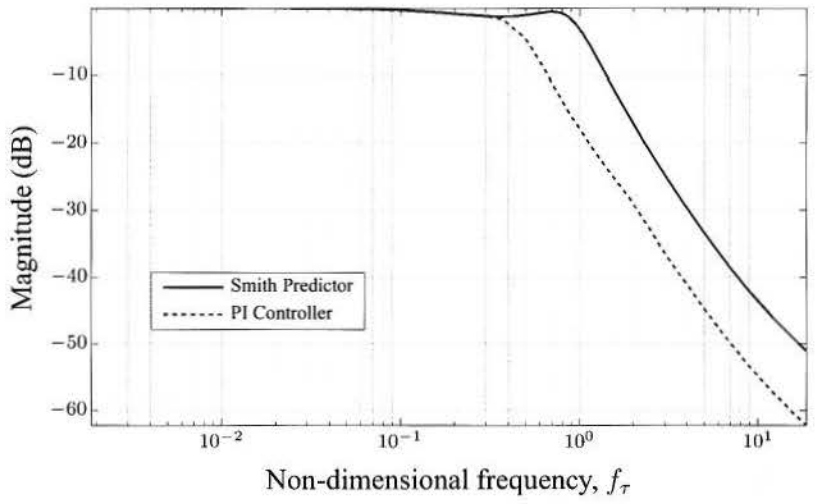

Figure 11.

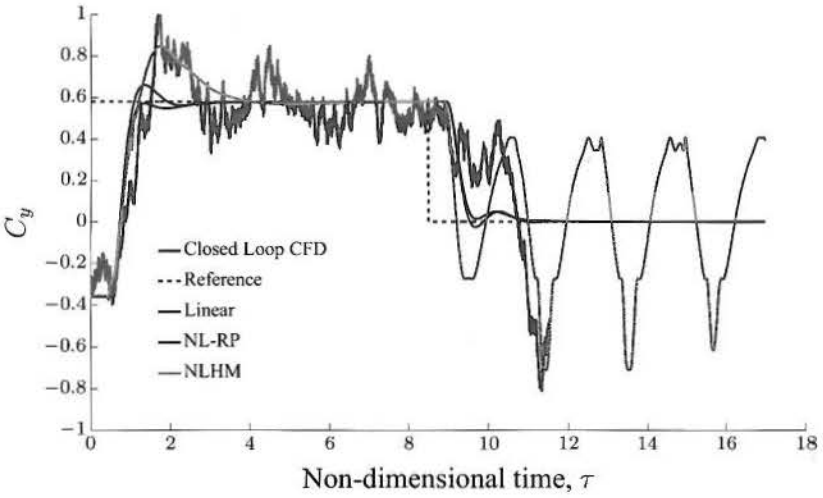

Figure 12.

implemented in the closed loop system and designed for adequate disturbance rejection and reference tracking performance. The closed loop transfer functions were analyzed. A time simulation was shown in which the controller was able to guide the asymmetric vortex state to an arbitrary asymmetric pressure distribution while adequately regulating the disturbances. The control was then validated in both experiment and Navier Stokes numerical simulations. Very good agreement existed between the two systems. The dynamics showed that frequencies larger than a flow though time could not be controlled. This is mainly due to the actuator placement at the nose of the axisymmetric body and the large convective time for a disturbance to reach the end of the geometric body. Also it is shown that the high frequency disturbance is mainly due to the separated shear layer along the side of the axisymmetric body. The modeling and understanding of the interaction between these primary vortices and the separated shear layer is critical for increasing the performance of flow control of an axisymetric body at high angle of attack.

References

[1] Deng, X., Wang, G., Chen, X., Wang, Y., Liu, P., and Xi, Z., "A physical model of asymmetric vortices flow structure in regular state over slender body at high angle of attack," *SCIENCE IN CHINA SERIES E-TECHNOLOGICAL SCIENCES*, Vol. 46, No. 6, DEC 2003, pp. 561–573.

[2] el Hak, M. G. and Ho, C.-M., "Unsteady Flow Around an Ogive Cylinder," *J. Aircraft*, Vol. 23, No. 6, 1986, pp. 520–528.

[3] Keener, E. R. and Chapman, G. T., "Side Forces on a Tangent Ogive Forebody with a Fineness Ratio of 3.5 at High Angles of Attack and Mach Numbers from 0.1 to 0.7," Tech. rep., NASA TM X-3437, 1977.

[4] Bridges, D. H., "The Asymmetric Vortex Wake Problem - Asking the Right Question," *AIAA Paper 2006-3553*, 2006.

[5] Deng, X. Y., Tian, W., Ma, B. F., and K.Wang, Y., "Recent progress on the study of asymmetric vortex flow over slender bodies," *Acta Mech Sin*, Vol. 24, 2008, pp. 475–487.

[6] Luo, S. C., Lua, K. B., and Goh, E. K. R., "Side Force on an Ogive Cylinder: Effects of Surface Roughness," *AIAA J.*, Vol. 39, No. 4, 2002, pp. 716–718.

[7] Ng, Y. T., Lim, T. T., Luo, S. C., and Lua, K. B., "Effects of Probe Interference on Side Force of an Inclined Ogive Cylinder," *J. Aircraft*, Vol. 42, No. 2, 2003, pp. 420–423.

[8] Darden, L. and Komerath, N., "Forebody Vortex Control at High Incidence using a Moveable Nose Stagnation Point," *AIAA Paper 1995-1775*, 1995.

[9] Bernhardt, J. E. and Williams, D. R., "Closed-Loop Control of Forebody Flow Asymmetry," *J. Aircraft*, Vol. 37, No. 3, 2000, pp. 491–498.

[10] Patel, M., Tilmann, C., and Ng, T., "Closed-loop missile yaw control via manipulation of forebody flow asymmetries," *J. SPACECRAFT AND ROCKETS*, Vol. 41, No. 3, MAY-JUN 2004, pp. 436–443.

[11] Bernhardt, J. E., *Closed-Loop Control of Forebody Flow Asymmetry*, Ph.D. thesis, Illinois Institute of Technology, 1996.

[12] Bernhardt, J. E. and Williams, D. R., "Proportional Control of Asymmetric Forebody Vortices," *AIAA J.*, Vol. 36, No. 11, 1998, pp. 2087–2093.

[13] Fagley, C., Porter, C., Seidel, J., Farnsworth, J., and McLaughlin, T., "Experimental Closed-Loop Flow Control of a von Karman Ogive at a High Angle of Attack," *31ST AIAA APPLIED AERODYNAMICS CONFERENCE*, 2013.

[14] Strang, W., Tomaro, R., and Grismer, M., "The Defining Methods of Cobalt60: A Parallel, Implicit, Unstructured Euler/Navier-Stokes Flow Solver," *AIAA Paper 1999-0786*, 1999.

[15] Karypis, G., Schloegel, K., and Kumar, V., *ParMETIS: Parallel Graph Partitioning and Sparse Matrix Ordering Library Version 1.0*, 1997.

[16] Fagley, C., Porter, C., Seidel, J., Farnsworth, J., and McLaughlin, T., "Optimal Sensor Arrangement for Asymmetric Vortex State Estimation on a Slender Body at High Incidence," *AIAA Aerospace Sciences Meeting, American Institute of Aeronautics and Astronautics, New Orleans, LA AIAA 2012-3046*, 2012.

[17] Lee, E., Lee, J., Lee, K., Seidel, J., Fagley, C., Porter, C., and McLaughlin, T., "Effects of the Plasma Actuation on the Asymmetric Vortex around an Ogive Body at High Incidence," *AIAA Aerospace Sciences Meeting, American Institute of Aeronautics and Astronautics, New Orleans, LA (submitted for publication)*, 2012.

[18] Farnsworth, J., Fagley, C., Porter, C., Seidel, J., and McLaughlin, T., "The Transient Response of a von Karman Ogive to Open Loop Plasma Actuation," *AIAA Paper 2012-2955*, 2012.

[19] Porter, C., Fagley, C., Farnsworth, J., Seidel, J., and McLaughlin, T., "Closed-Loop Flow Control of a Tangent Ogive at a High Angle of Attack," *AIAA Paper 2013-0395*, 2013.